

2014-05-01

# A Spiking Self-Organising Map Combining STDP, Oscillations and Continuous Learning

Rumbell, T

<http://hdl.handle.net/10026.1/5136>

---

10.1109/TNNLS.2013.2283140

IEEE Transactions on neural networks and learning systems

Institute of Electrical and Electronics Engineers (IEEE)

---

*All content in PEARL is protected by copyright law. Author manuscripts are made available in accordance with publisher policies. Please cite only the published version using the details provided on the item record or document. In the absence of an open licence (e.g. Creative Commons), permissions for further reuse of content should be sought from the publisher or author.*

# A Spiking Self-Organising Map Combining STDP, Oscillations and Continuous Learning

Timothy Rumbell, Susan L. Denham and Thomas Wennekers

**Abstract**—The self-organising map (SOM) is a neural network algorithm to create topographically ordered spatial representations of an input data set using unsupervised learning. The SOM algorithm is inspired by the feature maps found in mammalian cortices but lacks some important functional properties of its biological equivalents. Neurons have no direct access to global information, transmit information through spikes and may be using phasic coding of spike times within synchronised oscillations, receive continuous input from the environment, do not necessarily alter network properties such as learning rate and lateral connectivity throughout training, and learn through relative timing of action potentials across a synaptic connection. In this paper, a network of integrate-and-fire neurons is presented that incorporates solutions to each of these issues through the neuron model and network structure. Results of simulated experiments assessing map formation using artificial data as well as the Iris and Wisconsin Breast Cancer data sets show that this novel implementation maintains fundamental properties of the conventional SOM, thereby representing a significant step towards further understanding of the self-organisational properties of the brain while providing an additional method for implementing SOMs that can be utilised for future modelling in software or special purpose spiking neuron hardware.

**Index Terms**—Artificial neural networks, Neural engineering, Self organizing feature maps, Unsupervised learning.

## I. INTRODUCTION

**T**OPOLOGICALLY ordered spatial representations of features can be found in various sensory cortical areas [1], [2], such as ocular dominance bands [3], [4] and orientation maps [5], [6] in cat and primate primary visual cortex, a tonotopic map in the auditory cortex in cats [7], a gustotopic map in the primary taste cortex [8], an odor relationship representation in the olfactory bulb [9], a whisker map in the barrel cortex in rodents [10], [11], and a somatosensory map in the somatosensory cortex of primates [12]. Throughout development these cortical feature maps accrue several distinctive properties, such as disruptions that reflect actual discontinuities in the sensory periphery and disproportionate representation of early-developing portions of the receptor sheet [1]. The relationship between properties of the sensory input is reflected in the relationship between physical areas of cortex that are tuned to represent those properties [13], and the physical substrate of representation is capable of reorganising to a change in input properties [14], [15].

Manuscript received xxxx; revised xxxx

T. Rumbell, S. Denham and T. Wennekers are with the Cognition Institute, Plymouth University, PL4 8AA Plymouth, UK

Corresponding author: T. Wennekers, Tel.: +44 (0)1752 584917, Email: [thomas.wennekers@plymouth.ac.uk](mailto:thomas.wennekers@plymouth.ac.uk)

DOI:000000

The self-organising map (SOM) is a neural network algorithm inspired by the organisational structure of feature maps in the brain [16]. Throughout learning a SOM gradually maps statistical correlations present in a set of data onto a simple, low-dimensional, topological output representation. The discovery of features and feature relations in a complex space is also a goal of principal component analysis [17], and the combination of winner-takes-all competition and a neighbourhood function for learning allows generated representations to be sparse, orthogonalised, and analogous to the representations developed by clustering algorithms [18]. Learning in the SOM is unsupervised, making it useful in a variety of situations and easily modified to suit a variety of purposes (for a review of SOM applications, see [16], for recent examples of SOM modifications, see [19], [20]).

However, the SOM algorithm in its conventional form differs from the methods of learning and information coding present in cortical feature maps in several functionally important ways: biological neurons do not have direct access to global information, such as the distance of their weights from the current input data point relative to all other neurons in the layer, or the actual values of the current input data point, towards which their weights should be moved; information is transmitted in a sequence of post-synaptic potentials, often synchronised within and between layers [21], with coding of information in relative firing times contributing to rapid hierarchical processing abilities [22]–[24]; input enters the sensory periphery continuously, so must be converted from this stream into spike sequences; learning can be ongoing [25], without necessarily resorting to reductions in learning rate and neighbourhood width at prescribed intervals throughout training. The current work presents a series of modifications to the original SOM that addresses these issues while retaining functionality, thereby contributing towards understanding of the self-organisational properties of the brain while providing a SOM implementation that can be utilised for future modelling in software or special purpose spiking neuron hardware.

Temporal coding can be incorporated into the SOM by inserting spiking neurons in place of neurons that make weight comparisons or communicate through time-continuous gradual activity values. An influential model [26] consists of two layers of integrate-and-fire neurons. The first layer encodes input in the firing times of neurons in an array that collectively represent a real value. The second layer represents the SOM: the best matching unit is determined locally through integration of the input spikes; the neighbourhood function consists of local interactions through excitatory and inhibitory

connections. The network self-organises in an unsupervised manner according to a learning rule based on spike-timing, but makes use of a global reference time to establish weight adjustments. The reliance on globally available information makes the rule unsuitable for the current purpose. Additionally, the network is reset after each presentation of an input datum as it is unable to handle continuously presented input without this mechanism. Representative mappings of one- and two-dimensional input data are reported as a result suggesting that important functional properties of the SOM are present.

The network presented and analysed in sections II and III implements the principles of the SOM algorithm in a network of spiking neurons. Several features of the model are based in part on the model detailed above [26]. This spiking SOM can act as a base for future work, introducing additional biological constraints to replicate properties of the cortex. It can be used to help realise hardware and other technical applications of the SOM algorithm that can benefit from the use of temporal coding. Section II describes the model, explaining the combination of mechanisms used, and the method of evaluating output quality. Section III presents the results of testing the model, including extensive parameter analyses, demonstration of key features of the model and application to categorisation tasks. Finally, section IV summarises the work, discussing the current model in terms of its place within the field relative to existing models and its limitations.

## II. METHODS

The model described in this section is a two layer network of integrate-and-fire neurons similar to the model proposed in [26]. In both models, firing in the first layer encodes an actual data point as a temporal sequence of spikes. Neurons in the second layer respond as a result of this firing, and one of them will win the competition, i.e., fire first. Further firing in the second layer is influenced by lateral connections, representing the neighbourhood. Neurons physically close to the winning unit fire sooner due to stronger excitatory lateral influence, and neurons further from the winning unit fire later due to weaker excitatory or inhibitory lateral influence.

The current model differs from that of [26] by incorporating realistic post-synaptic potentials, spike-timing dependent plasticity, inhibitory control of the input layer to generate oscillatory behaviour (facilitating continuous input presentation through temporal segmentation), while allowing for continuous, on-going learning and stable neighbourhood size. The mechanisms controlling each of these aspects of the network will be detailed in this section. Parameters for the equations introduced below are listed in table I, in section III.

Simulations were conducted using custom made C software.

### A. Neuron Model

Leaky integrate-and-fire neurons were used for all neurons in the network, modelled by (1):

$$\tau_m \frac{dV}{dt} = I(t) - V + g\eta(t),$$

if  $V \geq \theta$  then spike and reset  $V = 0$  (1)

Each neuron has a membrane potential  $V$  that increases by integrating current input  $I(t)$ , and ‘leaks’ towards a resting potential of 0 when there is no input from its afferent synapses. The membrane potential time constant,  $\tau_m$ , is set to 1ms for all neurons in the model, except  $u_{Inh}$ , in which  $\tau_m = 0.5$ ms. A spike is generated when a neuron’s membrane potential reaches a firing threshold  $\theta$ , which varies by layer (see section II-C). Neurons are also subject to a Gaussian white noise process  $\eta$ , which is scaled by a factor  $g$ ;  $g = 0$  (i.e. no noise injection) for the majority of testing, but the robustness of network output to noise is tested by varying  $g$  in section III.

All connections between neurons are modelled synapses with weight  $w_{ij}$ , which transmit post-synaptic potentials (PSPs) to the post-synaptic neuron when a spike is generated in the pre-synaptic neuron. PSPs are modelled as  $\alpha$ -functions, using (2) and (3):

$$\tau_r \frac{ds_1}{dt} = (s - s_1) \quad (2)$$

$$\tau_f \frac{ds_2}{dt} = (s_1 - s_2) \quad (3)$$

where  $s$  is a binary value representing instantaneous presence or absence of a presynaptic spike,  $s_1$  is an internal state variable,  $s_2$  is the  $\alpha$ -function output, and  $\tau_r$  and  $\tau_f$  are time constants for the rise and fall duration of the response. Time constants are set independently for each layer (see table I), but the ratio of  $\tau_r:\tau_f$  is always set at 1:5.

Input current to a neuron at time  $t$ ,  $I(t)$ , is calculated by

$$I(t) = \sum_j w_j s_{2j}(t) \quad (4)$$

where  $w_j$  represents the connection weight (or synaptic efficacy) between neuron  $j$  (presynaptic) and the current neuron (postsynaptic), and  $s_{2j}(t)$  represents the current  $\alpha$ -function output from neuron  $j$ .

### B. Learning

The learning rule used in [26] makes use of some artificial features. Neurons have access to a global time stamp, which allows the gap between the firing time of the best matching unit and the firing time of the current neuron to be calculated. Also, the actual input value is compared with the current synaptic weight to determine the weight change, meaning that the synapse has knowledge of the input patterns. Replacing this learning rule with a standard spike-timing dependent plasticity (STDP) rule removes these issues, providing a basis for learning that is more biologically plausible [27], and more robust due to reliance only on local information to which each neuron already has access.

STDP [28] provides a function for long-term potentiation (LTP) or depression (LTD) of synapses based on the time difference  $\Delta t$  between a single pair of pre- and post-synaptic spikes, in neurons  $i$  and  $j$  respectively, according to  $w_{ij} \rightarrow w_{ij}(t) + f(\Delta t)$ . A linear multiplicative rule for LTD and exponential multiplicative rule for LTP are used, according to [29]:

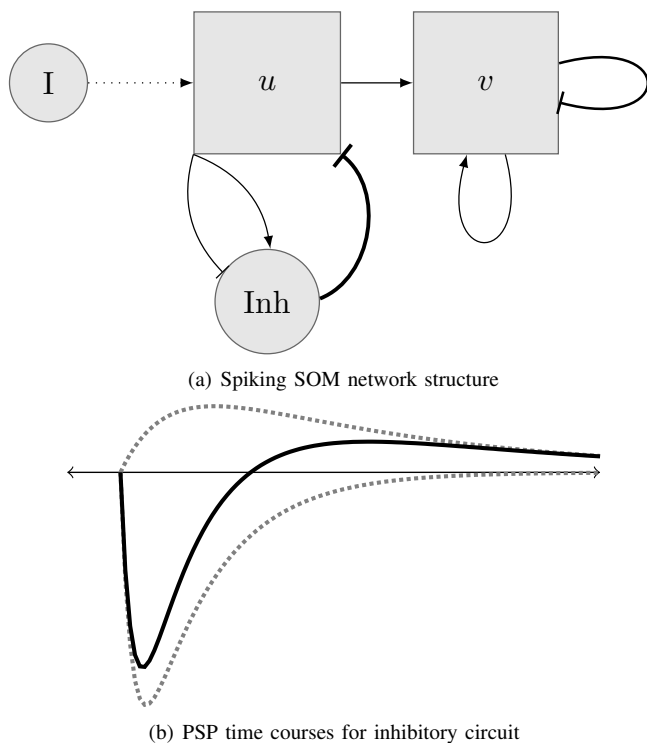


Fig. 1. (a) Spiking SOM network structure: an actual input value  $I$  is encoded into spikes times by nodes in layer  $u$ ; the inhibitory unit causes oscillations, allowing continuous input to be presented to  $u$  (see section II-C1 for details); feedforward connections from  $u$  to  $v$  drive firing in  $v$ ; early firing in  $v$  determines the location of output activity in  $v$  through lateral (neighbourhood) connections (see section II-C2 for details). (b) shows the time course of the post-synaptic potential from both of the  $u$  to  $Inh$  synapses (inhibitory is the lower dotted line, excitatory is the upper dotted line), together with the combined effect on the membrane potential of  $Inh_u$  (solid line)

$$f(\Delta t) = \begin{cases} \exp^{-w_{ij} A_+ (1 - \frac{1}{\tau_+}) \Delta t} & \text{if } \Delta t > 0, \\ -w_{ij} A_- (1 - \frac{1}{\tau_-}) \Delta t & \text{if } \Delta t \leq 0. \end{cases} \quad (5)$$

$A_+$  and  $A_-$  are both positive and determine the maximum amount of synaptic strengthening and weakening that can occur, respectively.  $\tau_+$  and  $\tau_-$  are time constants determining the range of time in which synaptic strengthening and weakening will occur, respectively. Weights are bounded between 0 and  $w_{max}$ . The specific values these five variables are set to, along with the motivation for differing forms of the rules for LTD and LTP, are discussed in section III-B, which details an extensive parameter search conducted to optimise learning.

### C. Network Structure

The spiking SOM network structure is shown schematically in Fig. 1. Conventional instantiations of the SOM receive input (numerical values for each dimension in the input data set) directly into the SOM neurons. In the spiking version presented here these values (represented by node  $I$ ) feed into a bank of neurons within an intermediate input layer,  $u$ . The actual input values are converted into a temporal spike sequence within each bank through the use of an inhibitory mechanism, described in section II-C1. This spike sequence then drives the SOM layer,  $v$ , through all-to-all feedforward

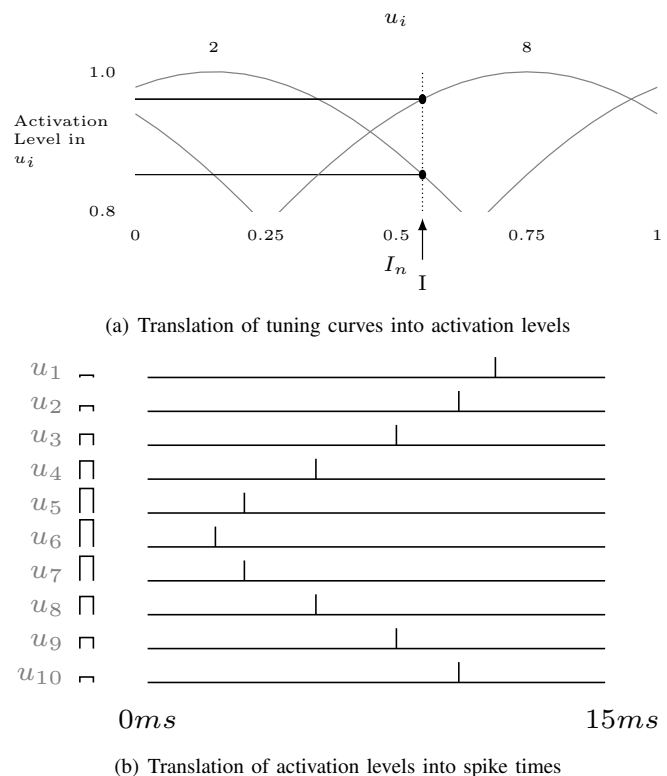


Fig. 2. Generation of a temporal sequence from a value in an input dimension and a bank of neurons tuned to points within that dimension. (a) shows the generation of an activation value for each neuron ( $u_i$ ) from within the bank of input neurons representing input dimension ( $I_n$ ). An example input value, at arrow  $I$ , of 0.55 is shown by the vertical dotted line. Activation values are established by the vertical point at which this dotted line crosses the tuning curve for a ( $u_i$ ) neuron. Example tuning curves are shown for neurons 2 and 8, tuned to values of 0.15 and 0.75 respectively. The vertical locations of the horizontal lines from this curve then represent the activation levels. (b) demonstrates the type of output firing sequence that results. The height of the bars shown next to each  $u_i$  represents the activation level generated from the intersection of a given input value and the neuron's tuning curve.

synaptic connections. All-to-all lateral synaptic connections in  $v$  implement the neighbourhood function.

1) *Input encoding within oscillations*: Input to this model is in the form of an  $m$ -dimensional vector of real numbers; each dimension  $I_n$  of this vector needs to be encoded in the firing of neurons in layer  $u$ . This can be achieved by representing each  $I_n$  with a bank of neurons  $u_n$  from layer  $u$ . Each neuron  $u_i$  in that bank is tuned around a point from within the range of values that  $I_n$  can take [30]. A Gaussian function is used such that the closer the actual value  $I_n$  is to the tuned value of  $u_i$ , the higher the activation to  $u_i$ , as shown in Fig. 2. The use of integrate-and-fire neurons means that  $u_i$  with higher activation levels will reach threshold earlier and fire faster than  $u_i$  with low activation levels. This creates a unique yet structured temporal pattern of spikes for each value of  $I_n$ .

Continuous stimulus presentation is an important feature in constructing a versatile and general network, allowing network operation to be ongoing, with no need for discretisation of temporal aspects, such as automatic resetting of the network state at each training step. Using the current method of input encoding, continuous input presentation provides constant

activation to layer  $u$ . This disrupts the temporal representation of each input pattern: the first  $u_i$  to fire will begin integrating input again first after resetting, and fire sooner in the next cycle of firing. This quickly desynchronises the input neurons from one another, meaning that information is encoded in the firing rates rather than the spike times.

This problem is remedied through an inhibitory neuron,  $Inh_u$ , which responds to firing in  $u$  with a slow inhibitory PSP fed back to all neurons in  $u$ . The inhibition depresses the membrane potential of all  $u_i$  after firing, establishing an approximate baseline for the effects of activation from  $I$ , creating a close to identical repetition of the temporal sequence. Inhibition in response to excitation creates an oscillatory behaviour, with a period of firing across the layer followed by a period of inhibition ahead of the next spikes. The temporal structure of spiking within each oscillation is maintained, meaning that information is now encoded in spike times rather than firing rates. Under the parameters in table I, inhibition in layer  $u$  commences 10-15ms after the start of firing in the layer, and the inhibitory PSP depresses membrane potentials sufficiently to prevent firing for approximately 10ms, when the temporal sequence begins again. This behaviour is shown between 15 and 30ms in the upper chart in Fig. 3, which shows the membrane potential time course for a sample  $u_i$ . This inhibitory effect could also be reached by a population of spiking neurons, but is simplified to a single neuron here. Furthermore, firing in  $v$  synchronises with oscillations in  $u$ , as the feedforward connections between the layers drive activity in  $v$ .

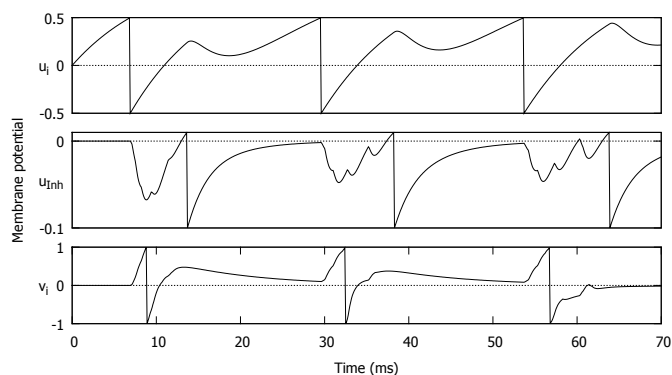


Fig. 3. Time course of membrane potentials in examples of the neurons  $u_i$  (top),  $u_{Inh}$  (middle) and  $v_i$  (bottom). Firing threshold is the top of the figure in each case. A membrane potential reaching threshold generates a spike and the membrane potential is reset, indicated by vertical lines in the figures. Potentials in layer  $u$  neurons increase, generating spikes, at which time the potential in  $u_{Inh}$  is depressed temporarily, due to the inhibitory connection from each  $u_i$ . The excitatory connections from each  $u_i$  then result in an increase in potential in  $u_{Inh}$ , which fires. This causes a temporary stagnation of the membrane potential in  $u_i$ , which would normally increase continuously due to continuous exposure to the actual input. The membrane potentials of neurons in layer  $v$  begin increasing after the onset of firing in  $u$ , some of which will spike (shown here) if they have strong weights to the early firing layer  $u$  neurons.

The inhibitory neuron receives input from each  $u_i$  through both an excitatory and an inhibitory synapse, as shown in Fig. 1(a). The excitatory synapse has a relatively long time constant, making it slow, and the inhibitory synapse has a

relatively short time constant, making it fast, as shown in Fig. 1(b). The overall effect of the pair of connections on the membrane potential of  $Inh_u$  is an initial dip, followed by a recovery into the positive region, shown in the middle chart of Fig. 3. Combined with a resting potential fractionally below the firing threshold, the effect is that the membrane potential of  $Inh_u$  will stay sub-threshold as long as there are spikes in  $u$  within a reasonably short time of each other, and then reach threshold when there is a sufficient gap in activity in  $u$ . As a result, membrane potentials in  $u_i$  are reset when there is a large gap in firing, or when the pattern ends.

In summary, oscillations are induced in the layer through excitatory followed by inhibitory firing, as in a classic excitatory-inhibitory feedback loop [31]. Oscillations of this type allow input neurons to be constantly excited and maintain a reliable firing pattern for an input. In turn, this allows for a stimulus, or input datum, to be continuously presented to the network, resulting in a versatile and reliable input coding mechanism.

2) *Neighbourhood function*: Self-organisation in the spiking SOM is produced through the use of a lateral interaction profile (analogous to a neighbourhood function), and STDP (see section II-B). Learning in the spiking SOM occurs when an output node fires in response to the input sequence; in particular, learning of the current input values is strongest when an output neuron fires soon after the start of the input sequence, causing greater strengthening of the afferent synapses from nodes that better represent the actual input values. Lateral synaptic connections in the output layer  $v$  send excitatory signals to neurons that are within a certain distance and inhibitory signals to more distant neurons. This lateral profile encourages neurons within a spatial region to fire and discourages neurons outside of that region from firing.

A suitable neighbourhood kernel, both in terms of capturing qualitative properties of cortical structure and functional properties of the SOM network, is a ‘Mexican-hat’ function [32]. Keith-Magee [33] discussed a lateral connection initialisation function for a SOM based on a Laplacian kernel

$$\bar{w}_{ij} = (1 + a)G(\|i - j\|, r) - aG(\|i - j\|, br) \quad (6)$$

in which the lateral connection strength  $\bar{w}_{ij}$  between output neurons at locations  $i$  and  $j$  in the grid is determined by (6), where  $a$  represents the magnitude of the negative component of the function,  $b$  determines the decay of the negative component of the function,  $r$  determines the radius of the positive component of the function, and the function  $G$  is a Gaussian function of the distance between  $i$  and  $j$ .

The traditional SOM formulation includes a decaying neighbourhood width over time to produce a more finely tuned output mapping. An appropriate decay function for the width ( $r$ ) of this lateral connection kernel is established, through a series of experiments [33], as a step function with a filter to smooth the step function over time:

$$r(t) = X - \frac{X - X'}{1 + (\sqrt{2} - 1)((T/t)^{2n})}. \quad (7)$$

where  $r(t)$  gives the value of  $r$  to use in (6) at training step  $t$  in the simulation,  $X$  and  $X'$  are values of  $r$  at the start and

end of training respectively,  $T$  represents the value of  $t$  that the 'step' is centred around, and  $n$  is the order, or amount of smoothing, of the 'smoothed step' function.

Compared with classic linear decay schemes and a non-smoothed step decay, use of (7) results in an accurate output mapping being reached more quickly [33]. Additionally, identical values for  $X$  and  $X'$  results in no neighbourhood decay, facilitating a simple transition between regimes.

The current spiking SOM model uses (6) and (7) to establish lateral synaptic weights. For a  $10 \times 10$  grid of neurons in layer  $v$ , parameter searching reveals that setting  $a$ ,  $b$ ,  $X$  and  $X'$  all to 3.0 provides a lateral connection profile capable of topological map formation. Identical values for  $X$  and  $X'$  lead to a constant  $r$  in (6); this was found to be capable of topological map formation, demonstrated in section III below, although it is possible that more accurate mappings can be obtained using a larger  $X$  and smaller  $X'$  [33]. This decision was made to ensure continuous learning in the output map, identified as a goal of the current system. Decay of neighbourhood size throughout training was utilised for results in sections III-F and III-G, however, and in these cases the step function in 7 was used to modify the lateral weights.

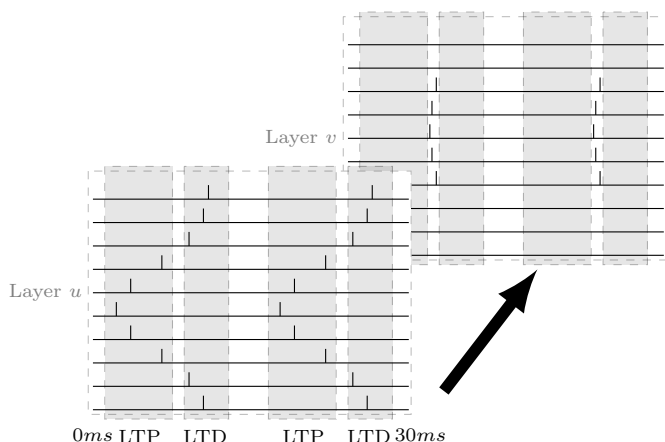


Fig. 4. The mechanics of self-organisation in the spiking SOM. A spike sequence in a bank of neurons in layer  $u$  represents the actual input value, with early firing neurons being well tuned to the actual value, and late firing neurons being poorly tuned to the actual value. The black arrow represents all-to-all feedforward synaptic connections from  $u$  to  $v$ . At some point in the firing of the pattern in  $u$ , a neuron in  $v$  fires, winning the competition and becoming the best matching unit. Neighbouring neurons in  $v$  are caused to fire within close temporal proximity. The gap between the LTP and LTD boxes in layer  $u$  represents the time at which firing in  $v$  occurs relative to the firing in  $u$ . Synapses from any neurons that have fired before that point are strengthened (the LTP box) and synapses from any neurons that fire after that point are weakened (the LTD box).

3) *Self organisation*: The inhibitory current generating an oscillation, the temporal coding of each input dimension in spike times, the neighbourhood function, and multiplicative STDP all contribute to the self-organisation of the output map. At the start of an oscillation the input neurons have depressed membrane potentials due to inhibition from the previous oscillation. Membrane potentials increase through constant input current and early spikes within an oscillation indicate neurons that represent the actual input well. Fig. 3 shows the relationship between these membrane potentials,

with a spike in a  $u_i$  leading to temporary depression of the membrane potential of the inhibitory neuron. The inhibitory neuron then fires, temporarily preventing the increase of the membrane potential of all  $u_i$ . This first part of the input firing pattern generates a spike in the output layer from the neuron best matching the input firing. This is followed by the firing of nearby output neurons due to lateral activity, all before firing of neurons in the input layer that are relatively poor representatives of the actual input. STDP causes the synaptic connections from neurons in the early part of the input pattern to be strengthened, and the later part of the input pattern to be weakened, for output neurons within the neighbourhood of the winning neuron. This is illustrated schematically in Fig. 4.

A multiplicative form of STDP helps to ensure that weights reach a stable point roughly proportional to how often an input neuron fires before an output neuron relative to how often it fires after an output neuron. Output neurons will respond for actual input values that are a distance away from their preferred input value, due to lateral excitation. As such, weights will be increased at synapses from input neurons that normally fire after the output neuron in the output neuron's preferred input pattern. Weights will be decreased from input neurons that normally fire before the output neuron in the output neuron's preferred input pattern. These changes are weight dependent, so for a certain weight value a few instances of depression balance with a greater number of instances of excitation, and vice versa, creating stability. This stability means that there can be precise differentiation between winning output neurons; adjacent output neurons will prefer similar input neurons, so stable weights between the maximum and minimum are important in determining which of several neurons with similar preferences reaches threshold first.

#### D. Quality of map formation metric

The ability of a SOM to map an input data set can be assessed by checking the topographic mapping error of the output map given the input data. For a map with no mapping error, the relative distance between any pair of data in the input space is the same as the relative distance between the locations activated by that pair of input data in the output map. Metric Multidimensional Scaling (MDS) can be used to assess this, according to

$$E_{MDS} = \sum_{i=1}^N \sum_{j < i} (F(i, j) - G(M(i), M(j)))^2 \quad (8)$$

where  $N$  is the number of input patterns,  $F(i, j)$  represents the actual dissimilarity of the pair of input patterns  $i$  and  $j$  (measured as Euclidean distance), and  $G(M(i), M(j))$  represents the dissimilarity between the locations in the output map representing patterns  $i$  and  $j$  (measured as Euclidean distance), where  $M(i)$  and  $M(j)$  are the locations of the winning nodes in layer  $v$  for input patterns  $i$  and  $j$  respectively [34]. The value of  $E_{MDS}$  represents how well the final network mapping preserves the topology of the input data set. The most accurate mapping achieved is one in which relative distances between patterns in the input space are reflected exactly by relative

distances between neurons representing those patterns in the output space, resulting in a minimum  $E_{MDS}$  value of 0. The least accurate mapping seen in practice is one in which all input patterns result in activation of the same location in the output map; the  $E_{MDS}$  value for this situation will vary depending on the distribution of input patterns. This test is used in [26] to analyse their spiking SOM, with final  $E_{MDS}$  values of under 20% of the starting value being reported. Values in section III are reported using mean values for  $E_{MDS}$ , with the final summed  $E_{MDS}$  divided by the total number of pairs of input patterns compared, to give a value that can be compared regardless of the number of patterns in the input space.

Alternate methods for analysing the quality of output mapping produced by a SOM are available (see [34]–[36] for reviews). MDS has been selected as an analytical tool ahead of other techniques for two primary reasons. First, it meets two criteria proposed by Polani [37] that are required for a SOM analysis tool: it should provide evidence of the self-organising process during training (shown through a reduction in error value); and it should measure the embedding of the set of neurons into the data manifold (the error value measures how well changes in the input space are mapped by changes in the output space). Second, given that it represents an appropriate SOM analysis tool, it is important that results described here are generalisable for potential comparison with other spiking neuron network implementations. Other spiking neuron networks may not be specifically designed as SOM implementations, and specific SOM analysis metrics would lose their relevance when comparing the topographic mapping capabilities of one spiking neuron network with another.

### III. RESULTS

This section covers the results of testing conducted to confirm the behaviour of the spiking SOM. A measure of the quality of map formation is introduced in section II-D, to be used to interpret the rest of the testing results. The parameters used during testing are described in section III-A, and a parameter search on the variables involved in (5) is described in section III-B, to determine the range of values that result in good map formation. Section III-C demonstrates the robustness of learning under the chosen parameters in the presence of noise. The spiking SOM has been tested in common scenarios used to test the conventional SOM: the response of the spiking SOM to evenly distributed, randomly selected, two-dimensional input data is analysed in section III-D. Finally, the results of categorisation tests carried out with the spiking SOM are reported in sections III-E, III-F and III-G.

#### A. Network parameters

The testing conducted in sections III-B and III-D made use of standardised parameters for the network, shown in table I. In summary, each dimension  $n$  in the input  $I$  was associated with a bank  $u_n$  of 10 neurons in layer  $u$ . The value of  $n$  was set to 2 for two-dimensional input. The preferential values of the neurons in each  $u_n$  were equally spaced between 0.05 and

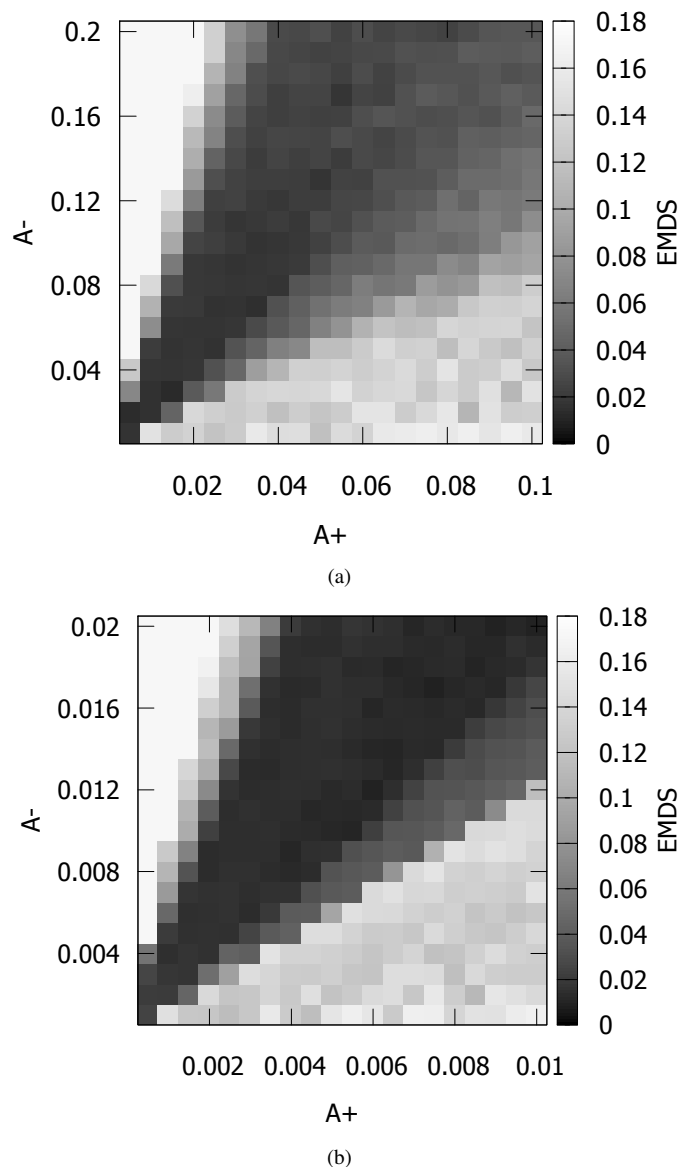


Fig. 5. Parameter search results for  $A_+$  to  $A_-$  values: normalised final  $E_{MDS}$  values averaged from 30 trials are presented, for ranges of  $A_+$  and  $A_-$  values at low resolution (a) and at high resolution (b)

0.95. Gaussian tuning curves around these preferential points were used for calculation of the activation values, with distance calculations including circular wrapping from 1 to 0.

Layer  $v$ , the SOM layer, was initialised with 100 neurons, arranged in a  $10 \times 10$  grid through the lateral connection weights. Feedforward connections were initialised from all layer  $u$  neurons to all layer  $v$  neurons with a randomised weight between 0.4 and 0.6 of the maximum synaptic weight  $w_{max}^{u \text{ to } v}$ . The radius  $r$  (in (6)) was set to 3.0, and the distance between neurons in the layer were calculated with toroidal structure. Values of  $\tau_+$  and  $\tau_-$  in (5) were set to 11ms and 10ms respectively. This width of learning window approximately matches the temporal width of a network oscillation, leading to negligible influence on learning of spikes from within neighbouring oscillations.

At the start of each training step an input value was

determined by selecting randomly from 10 values for each dimension, equally spaced between 0.05 and 0.95, making a total of 100 input patterns from within the two-dimensional input space. A training step lasted through 5 oscillations of the network (approximately 125ms) before the input pattern was changed. The network was allowed to learn for 4000 training steps. Quality of map formation was assessed using mean  $E_{MDS}$  for each pair of input patterns. Given that for the two-dimensional case both the input and output space wrap toroidally, this situation results in a maximum mean  $E_{MDS}$  value of  $\frac{1}{6}$ .

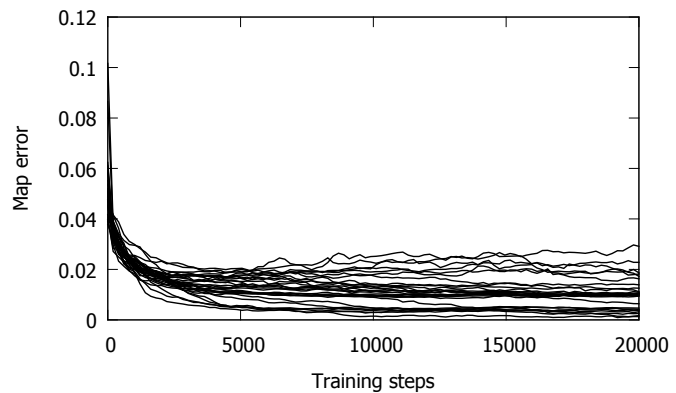
The maximum connection strength values for synapses with presynaptic neurons in layer  $u$  are varied for the categorisation tests conducted in sections III-F and III-G. These datasets contain four and nine input dimensions, resulting in 40 and 90 neurons in  $u$ , respectively. As such, the value of  $w_{max}^{u \text{ to } v}$  is scaled down to 1.5 in section III-F, and 0.7 in section III-G, and the  $w_{max}^{u \text{ to } Inh^u}$  values to 0.4 in section III-G.

### B. Learning parameter analysis

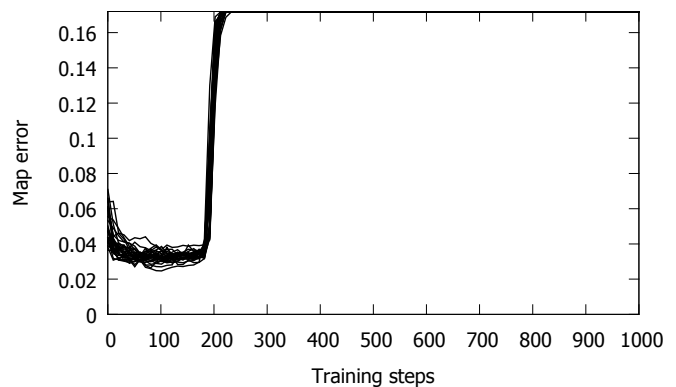
Parameter testing was conducted to establish suitable values for the maximum and minimum weight change parameters,  $A_+$  and  $A_-$  from (5). A test of a parameter set consisted of 30 randomly initialised maps, trained using the method described in section III-A involving random selection from 100 input patterns evenly spaced across the 2D surface. An average normalised  $E_{MDS}$  value taken at the end of training used to gauge the quality of maps formed with those parameters. Coarse- and fine-grained searches were conducted, the results of which are shown in Fig. 5(a) and 5(b) respectively.

The fine-grained search results establish that, for a range of  $A_+$  values up to 0.01, and  $A_-$  values up to 0.02, a ratio between 1:2.5 and 1:3.5 of  $A_+$  to  $A_-$  will result in good map formation. The coarse-grained search result establishes that there is little performance degradation up to  $A_+$  values of 0.045 and  $A_-$  values of 0.11, meaning that large weight changes relative to the maximum weight can still result in map formation. Only 500 training steps were used in the coarse-grained simulation results; the high learning rates involved result in a fluctuating error value after this point, rather than increased convergence of error values.

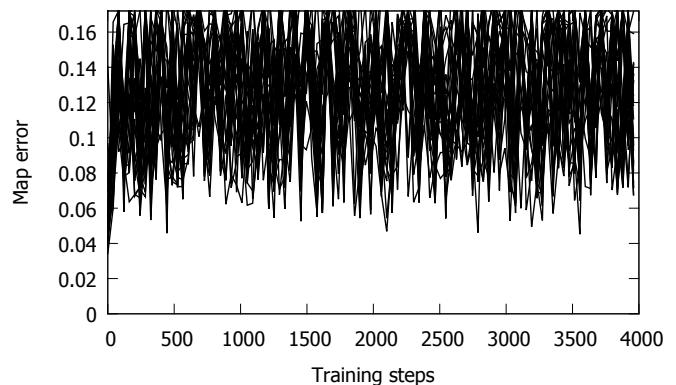
Fig. 6 shows the progression of  $E_{MDS}$  values throughout training for important locations in the parameter space. Fig. 6(a) shows the mapping error attained for multiple trials for an  $A_+$  to  $A_-$  ratio of 1:3.5, a ratio that reliably results in good map formation. Fig. 6(b) shows the degradation of map quality for an  $A_+$  to  $A_-$  ratio of 1:20. Depression dominates, and weights are gradually lowered until activity in  $u$  no longer evokes any spikes in  $v$ . If no neurons win the competition for any input pattern, there is no distance between winning nodes for any input pattern, so a maximum error value is reached. This outcome is characteristic of all  $A_+$  to  $A_-$  ratio smaller than 1:6. Progression of error values throughout training for the opposite situation, a dominance of potentiation, is shown in Fig. 6(c), with an  $A_+$  to  $A_-$  of 4:1. In this regime, there is too little depression of weights for connections from input neurons representing less preferred input patterns, eventually resulting



(a) Normal learning



(b) Dominance of depression



(c) Dominance of potentiation

Fig. 6. Time course of  $E_{MDS}$  values for 3 points in the parameter space, representing: (a) normal learning ( $A_+ = 0.002$ ,  $A_- = 0.007$ ); (b) dominance of depression ( $A_+ = 0.0005$ ,  $A_- = 0.01$ ); and (c) dominance of potentiation ( $A_+ = 0.02$ ,  $A_- = 0.005$ );

in one output region of the map dominating for all input patterns. Wild fluctuations are seen in the error value; this is caused by slightly different neurons, still close to the dominant region, winning the competition for different input patterns. A brief change in winning neuron can result in a temporary large variation in error value. This outcome is characteristic of all  $A_+$  to  $A_-$  ratio greater than 1:1.

For the following simulations, an  $A_+$  value of 0.0016 and an  $A_-$  value of 0.0055 will be used. These values are situated within the acceptable ratio of these parameters, and represent

TABLE I  
 NETWORK PARAMETERS FOR ALL SIMULATIONS DESCRIBED IN SECTION III

(A) Neuronal parameters, used in (1) and (4)									
$\Delta t$	$\tau_m^{u,v}$	$\tau_m^{Inh u}$	$V_{rest}$	$\theta^u$	$\theta^{Inh u}$	$\theta^v$	$g$		
0.1ms	1ms	0.5ms	0.0	0.5	0.01	1.0	0.0		
(B) Synaptic parameters, used in (2) and (3) for different synapse types									
$u$ to $v$		$u$ to $Inh u$ (exc.)		$u$ to $Inh u$ (inh.)		$Inh u$ to $u$		$v$ to $v$	
$\tau_r$	$\tau_f$	$\tau_r$	$\tau_f$	$\tau_r$	$\tau_f$	$\tau_r$	$\tau_f$	$\tau_r$	$\tau_f$
0.2ms	1.0ms	0.4ms	2.0ms	0.2ms	1.0ms	1.0ms	5.0ms	0.1ms	0.5ms
(C) Maximum magnitudes of synaptic connection strength									
$w_{max}^{u to v}$	$w_{max}^{u to Inh u (exc.)}$	$w_{max}^{u to Inh u (inh.)}$	$w_{max}^{Inh u to u}$	$w_{max}^{v to v}$					
2.2	1.0	1.0	100.0	1.0					
(D) Neighbourhood parameters, used in (6) and (7), for layer $v$									
$a$	$b$	$X$	$X'$						
3.0	3.0	3.0	3.0						
(E) Learning parameters, used in (5)									
$A_+$	$A_-$	$\tau_+$	$\tau_-$						
0.0016	0.0055	11ms	10ms						

a low learning rate compared to the maximum acceptable rate.

### C. Robustness to noise

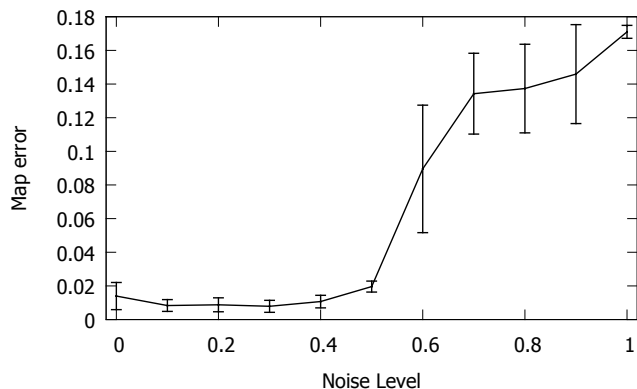


Fig. 7. Average  $E_{MDS}$  value after training plotted against the value of variable  $g$ , magnitude of noise in the neuron model. Error bars represent 1 standard deviation. Accuracy of the output mapping stays high until noise levels reach a critical point around 0.5, with accuracy of the final mapping ending up close to the maximum error value as  $g$  reaches 1.

The noise scaling factor  $g$  was tested for 11 values between 0.0 and 1.0, with the same value used for both layers  $u$  and  $v$ , to analyse the robustness of the SOM formation to variable spike times. These values of  $g$  resulted in spike time variations in the input pattern of up to around 3ms. Other network parameters, input data set and input pattern selection remained as described in III-A and used in III-B. Fig. 7 shows average  $E_{MDS}$  values for training with variation in  $g$ . The average values of  $E_{MDS}$  ranged from 0.008 to 0.020 for values of  $g$  up to 0.5, and between 0.090 and 0.146 for  $g$  from 0.6 to 0.9, showing that noise in the neuron model does not prevent the learning mechanism from picking up the statistical correlations present in the input data until a value of  $g$  greater than 0.5.



Fig. 8. Final  $u$  (y-axis) to  $v$  (x-axis) synaptic weights after training with 2-dimensional data (light represents a strong connection and dark represents a weak connection; the top half of the graphic is the bank of input neurons encoding the first dimension and the bottom half is the bank encoding the second dimension; and each ten steps along the x-axis represents a row of output neurons, then the next ten represent the next adjacent row, and so on): the connections to the output layer vary in one dimension across an individual row (with consistency throughout the map), and vary in the other dimension across the rows, encoding the current input as a location in the output map in an organised way. A change in one input dimension (the bottom 10 rows) as one moves through each row of the output layer (each block of 10 columns), and a change in the second dimension (the top 10 rows) as one moves down through rows in the output layer (changes between each block of 10 columns in the figure) can be seen. For a given output neuron (one column), a gradual decrease in weights either side of a central point in each input dimension is visible.

### D. 2D input

A test often applied to SOM algorithms is to present random samples from a range [0,1] in two dimensions as input to the network, and test the ability of the output to organise itself into a formation capable of representing this input data.

An average final normalised  $E_{MDS}$  value of 0.00554 was achieved, over 64 trials (standard deviation 0.00483). The final weight matrix for the feedforward connections from input to output neurons is shown in Fig. 8; neurons in one row of the output layer are strongly connected to a specific range of input neurons in one dimension, while varying their connection strength to input neurons in the other dimension uniformly across the row (with the inverse pattern seen within and between columns). Fig. 9 displays the output layer neurons as circles, with nearest neighbour connections indicated by connecting lines, positioned in the input space according to the input value to which they respond most quickly (i.e., are

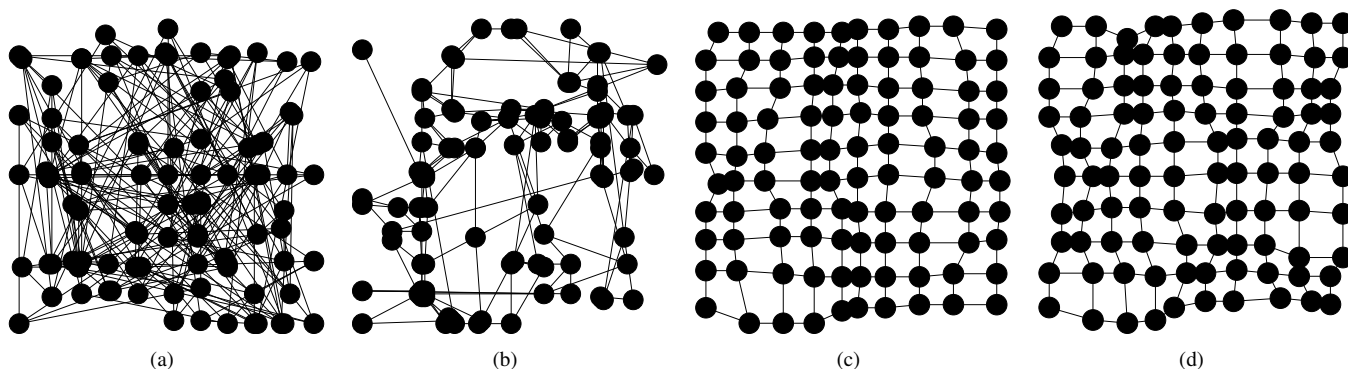


Fig. 9. Representation of  $u-v$  feedforward weights in the 2-dimensional input space, where black dots represent output layer neurons and black lines represent nearest neighbour synaptic connections (input and output dimensions are toroidal, but nearest neighbour edges to opposite sides of the input space are omitted for clarity of the figure). (a) shows the random starting distribution; after 200 training steps (b) the nodes begin to align to the input data; (c) and (d) show the trained map after 2800 and 3600 training steps respectively - learning is ongoing, so stochastic fluctuations in the distribution of recent input patterns are reflected by minor modulations in the map weights.

best tuned to); this preferential tuning is initially random, and throughout training organises to mirror the inputs received. It is worth noting that Fig. 9(c) and Fig. 9(d) both show the network state after a good mapping has been achieved, but the position of the neurons is quite variable; this is because the network is learning at the same rate throughout training in this example, and will morph slightly depending on the distribution of the most recent input data.

The spiking SOM is also capable of generating a map representation skewed to fit the input distribution. To test this the map was trained using six distributions of two-dimensional input data. In each distribution the likelihood of either dimension being drawn from the range  $[0,0.5]$  was altered to a value in the range of  $[0,0.5]$  at increments of 0.1. A likelihood of 0.5 represents an even distribution across the two-dimensional space, and a likelihood of 0 represents a distribution entirely in the quadrant of the two-dimensional space between 0.5 and 1.0 in both dimensions. Within each half of each dimension, the distribution is even across the range. The representation of the output nodes in the input space is shown in Fig. 10, as in Fig. 9. In Fig. 10(a) - Fig. 10(d) the input distribution can effectively be split into quadrants of likelihood. At any training step the input pattern is least likely to be selected from the lower-left quadrant (between 0 and 0.5 in both dimensions), most likely to be selected from the upper-right quadrant (between 0.5 and 1 in both dimensions), with each of the remaining quadrants at an intermediate likelihood (between 0 and 0.5 in only one dimension). Discontinuities can be seen in the map representation in Fig. 10(d); these are at the boundaries of the toroidal space, and are actually adjacent such that the extended sections on the top are interlocked with the gaps at the bottom. Fig. 11 demonstrates that map formation on average results in good representations of input distributions by the proportion of nodes in the final output mapping that represent a quadrant of the input space.

Another feature of the mapping shown by some SOM algorithms that attempt continuous learning is the ability of the network to reconfigure to a new input distribution midway through training, after a mapping has been established to an existing input distribution. This was tested by training the

network using only 75% of the input data space, leaving out the quarter of the input space square covered by values of greater than 0.5 in both dimensions. This reduced data set was used for 2000 training steps, then the full range of input data, including the previously omitted quarter, was used for a further 2000 training steps.

The evolution of the topographic error (Fig. 12) shows that the network adjusts to the initial input range as normal, but settles at a slightly higher  $E_{MDS}$  value, most likely due to the discrepancy between shape of input space and shape of lateral connections in the output layer. The extra data is introduced half way through training, resulting in a spike in  $E_{MDS}$  value, as the output mapping is no longer suitable for the input data, and the error is then reduced to a lower value as the output map reorganises to the new data. The mapping of the output nodes in the input space is shown in Fig. 13. The output nodes map to the original input space during the first half of training, and reorganise in the second half such that the final mapping is qualitatively identical to that seen in Fig. 9. The final weight matrix for the feedforward synapses is also qualitatively identical to the one obtained when training using the full data range from the start (Fig. 8). This simulation demonstrates that the map has learnt to represent the initial input distribution, but when a new distribution is presented the map is capable of adjusting appropriately.

### E. Categorisation

SOMs can cluster input patterns, creating a specific spatial location that is activated by incoming members of a specific category. If there are category divisions in the input data, nodes in the output layer will respond more reliably to one category of input than to others. A trained SOM can therefore be used as a categorisation tool by assigning each output node a category to represent based on whether that node fires reliably for one particular category. The capacity of the spiking SOM to be used as a categoriser in this way has been tested through training with two datasets commonly used for assessing the categorisation ability of a system. This capacity is demonstrated to provide evidence that organisation to datasets that contain relatively distinct categories within a high-dimensional

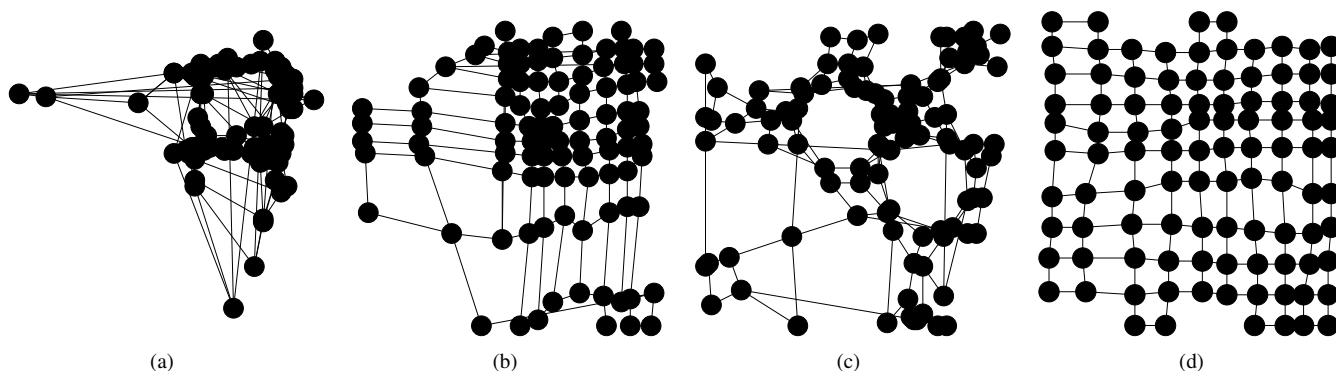


Fig. 10. Representation of  $u$ - $v$  feedforward weights in the 2-dimensional input space, where black dots represent output layer neurons and black lines represent nearest neighbour synaptic connections (input and output dimensions are toroidal, but nearest neighbour edges to opposite sides of the input space are omitted for clarity of the figure; neurons on the map border are alternating from one side of the figure to the other because the toroidal nature of the input space means that input values of 0 and 1 are essentially identical, and the row or column that the neurons are a part of is lined up along the 0-1 divide, with some neurons placed just on one side and some just on the other). (a), (b), (c), (d) show the final mapping for input distributions in which the probability in both dimensions of an input value being between 0 and 0.5 is 0.1, 0.2, 0.3 and 0.4 respectively.

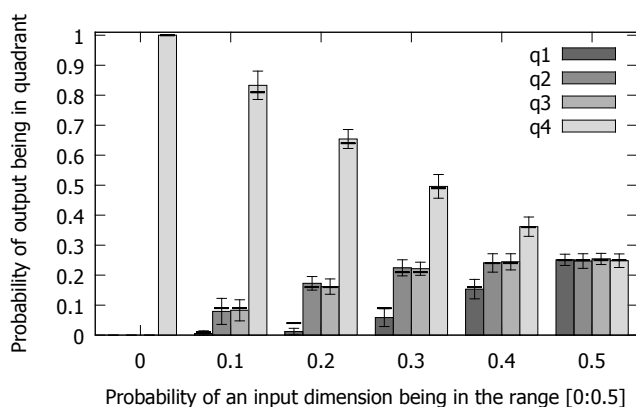


Fig. 11. The probability of an output node in a trained map representing each quadrant of the input space, plotted against the likelihood of an input dimension having a value within the range  $[0,0.5]$ . Bar height represents average over 30 trials; error bars represent standard deviation; black horizontal marks represent the actual probability of an input datum being within a quadrant of the input space; q1, q2, q3 and q4 represent the lower left, upper left, lower right and upper right quadrants respectively.

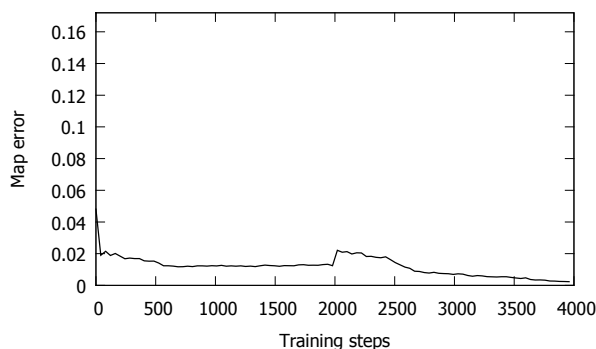


Fig. 12. Typical evolution of average  $E_{MDS}$  value for 2-dimensional input: the error in the output map reduces up to the halfway point in training, at which point the input distribution is expanded; the error in the map jumps up as the error measure is now relative to the new distribution; the error then decreases again as the map adjusts to the new distribution.

space is possible using this network, alongside representations of less discrete input data.

In the examples in sections III-F and III-G five-way cross validation is performed: a dataset is split into 5 chunks and the network is initialised and trained 5 times, using a different set of 4 chunks as training data and 1 chunk as testing data each time, so that in total all data points are used for testing once. Each training phase lasted for 4000 training steps with random selection of input pattern after each 5 oscillations of the network, as described in section III-A. At the end of a training phase the output nodes were designated as representing a category based on the input category to which they responded most frequently during training. The testing patterns were then presented to the trained network one at a time, and the output activity recorded. Lateral connections were still used in this testing phase, so multiple neurons in the output layer fired for each testing pattern, in an area with width determined by the lateral connection profile at the end of the training phase. The testing pattern was categorised by the network as belonging to the category to which the highest number of output neurons firing in response to that input pattern had been designated as representing. If more of the output neurons firing in response to a testing pattern had been designated with that pattern's category during the training phase than any other single category, then the pattern was considered to have been correctly classified.

#### F. Iris dataset

The first dataset used to test the categorisation performance of the spiking SOM was the Iris dataset [38]. This dataset is of sizes of flowers of the Iris plant; it consists of three categories each with 50 members, and each data point has 4 values, petal length, petal width, sepal length and sepal width. One of these categories "Iris Setosa Canadensis", is fairly distinct from the other two, "Iris Virginica" and "Iris Versicolor".

For the current purpose, the values for each dimension were normalised in the range  $[0-1]$ , and the spiking SOM model was initialised as in section III-D but with 40 input neurons, making one bank of 10 for each dimension. This increase

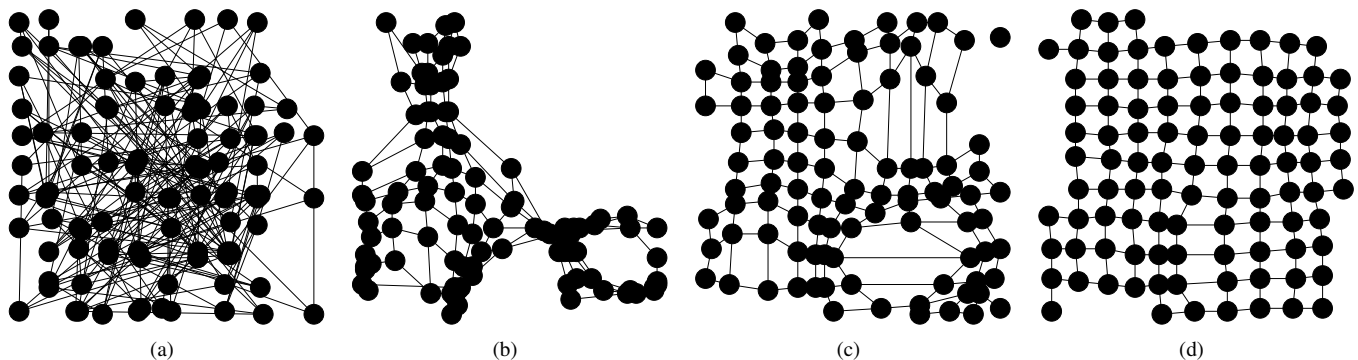


Fig. 13. Representation of  $u$ - $v$  feedforward weights in the 2-dimensional input space (arranged as per Fig. 9): (a) shows the random starting distribution; after 8000 training steps with the partial input data (b) the nodes are aligned to the input data space, leaving a gap in the input space from which no training examples have yet been received; (c) shows the expansion of the map to the newly increased range of input data after 800 training steps with the full input distribution; and (d) shows the trained map after 2000 training steps with the full data range - the map has adjusted to the new input data.

TABLE II  
CATEGORISATION ACCURACY (%) OF SPIKING NEURON AND NON-SPIKING NEURON ALGORITHMS FOR THE IRIS DATASET. THE CURRENT APPROACH IS SHOWN AS SPIKING SOM WITH NEIGHBOURHOOD REDUCTION (NR) AND SPIKING SOM WITHOUT NR.

Non-spiking	% acc.	SpikeProp [39]	% acc.
k-Means [30]	88.6	RBF [30]	92.6
SOM [30]	85.33	SpikeProp [39]	96.1
Matlab BP [40]	95.5	SWAT [40]	95.3
Matlab LM [40]	95.7	RBF [41]	89
TEST [42]	91.7	SNN <sub>Bako</sub> [43]	83.4
		Spiking SOM with NR	90.9
		Spiking SOM without NR	87.8

in number of input neurons meant that the feedforward connection strength from layer  $u$  to layer  $v$  had to be reduced; the value of  $w_{max}^{utov}$  was scaled down to 1.5. Remaining parameters remained identical, with the exception of the  $X$  and  $X'$  values in (7), controlling the evolution of the width of the neighbourhood function. For continuous learning these values are identical, meaning no change in lateral connection strengths over time. The standard neighbourhood parameters were used as one condition in the categorisation performance tests ( $X=3.0$  and  $X'=3.0$ ). However, output map quality can potentially be improved by starting with a large neighbourhood and reducing it throughout training. This approach can obtain a globally ordered topology initially, and refine details later on. This regime was used as a second condition in the categorisation tests, with  $X$  set to 4.0 and  $X'$  to 2.5. These values are in numbers of neurons, so for a  $10 \times 10$  map a radius of greater than 4.0 is the majority of the map.

Categorisation accuracy, averaged over 9 trials, was 87.8% (standard deviation = 1.3%) in the without-neighbourhood-reduction condition, and 90.9% (standard deviation = 1.7%) in the with-neighbourhood-reduction condition. Table II shows these results in comparison with the results achieved for other categorisation algorithms using this dataset. The spiking SOM categorises better than Matlab implementations of the k-Means and SOM algorithms [30] (although parameters used and the extent of parameter searching conducted to achieve these

TABLE III  
CATEGORISATION ACCURACY (%) OF SPIKING NEURON AND NON-SPIKING NEURON ALGORITHMS FOR THE WBC DATASET.

Non-spiking	% acc.	SpikeProp [39]	% acc.
Matlab BP [40]	96.3	SWAT [40]	95.3
Matlab LM [40]	96.7	SNN <sub>Bako</sub> [43]	89.5
		Spiking SOM with NR	96
		Spiking SOM without NR	97

results are unclear), the FPGA implemented classification network of [43], and the spiking neuron RBF network of [41].

Categorisation performance is slightly worse than several other networks: the spiking RBF model of [30], the SpikeProp model of [39], the SWAT model of [40], the TEST algorithm [42], and Matlab implementations of the backpropagation and Levenberg-Marquardt training algorithms [40]; it is worth noting, however, that these are designed specifically for data classification purposes, and do not feature the topographical ordering properties of the SOM model.

### G. Wisconsin Breast Cancer dataset

The second dataset used for categorisation testing was the Wisconsin Breast Cancer dataset (WBCD), consisting of 683 samples from 2 categories (444 benign and 239 malignant tumours), with 9 measures of features of cytology. Each of the 9 measures is a discrete value from 1-10, converted into a value in the range 0:1 for the current purpose, and represented using a bank of 10 input neurons, meaning that layer  $u$  consisted of 90 neurons. As such the value of  $w_{max}^{utov}$  is scaled down to 0.7, the value of  $w_{max}^{utoInhu}$  to 0.4, and the  $X$  and  $X'$  values were adjusted to 3.5 in the without-neighbourhood-reduction condition, to account for only having 2 categories occupying the  $10 \times 10$  output map; all other parameters remained identical to those used in section III-F.

Categorisation accuracy, averaged over 8 trials, was 96.4% (standard deviation = 0.4%) in the without-neighbourhood reduction condition and 97.0% (standard deviation = 0.1%) in the with-neighbourhood reduction condition. Again, these results are compared with the categorisation accuracy of other

algorithms using this dataset, shown in table III. The spiking SOM again outperforms the FPGA categorisation algorithm implementation of [43], and achieves a very similar level of accuracy to models that have been designed specifically for clustering and categorisation operations.

#### IV. DISCUSSION

The spiking neuron SOM model implemented here has been demonstrated to produce qualitatively and quantitatively similar output to the traditional SOM algorithm. This implementation combines continuously presented input, regular oscillatory firing, phase coding of input values,  $\alpha$ -function PSPs, leaky integrate-and-fire neurons, and STDP. The current model exhibits good categorisation performance for generic datasets without resorting to additional fine-tuning of parameters. Furthermore, it can function similarly to the traditional SOM algorithm without necessarily decaying learning rate or neighbourhood size throughout training. This section contains a set of comparisons of the current model with related existing approaches (section IV-A), and a discussion of some novel aspects of the mechanisms used, and limitations of those within the current model (IV-B).

##### A. Related approaches

The current model improves on the spiking SOM model of [26], described in section I, in several significant ways. The incorporation of continuous input and oscillatory firing means that the current network does not need resetting. The change to STDP for learning and introduction of  $\alpha$ -function PSPs both contribute to an improvement in the biological plausibility and performance of the model. Additionally, testing has established the robustness of the new approach to changes in the learning parameters, noise, and input data.

Other SOM-like networks have been implemented using spiking neurons. In [44] a two layer SOM structure similar to [26] made up of 'MacGregor' neurons [45] is used to test a pair of Hebbian learning rules, one with learning based on strength of PSPs and the other based on temporal correlations. It is demonstrated that, with an appropriate lateral connection neighbourhood, either of these learning approaches can result in output space segregation that is related to properties of the input space. However, properties of the conventional SOM such as smooth mapping of input to output space and categorisation are not demonstrated. Additionally, this model does not process continuous input, encode specific input values in temporal sequences, or utilise oscillatory behaviour.

In [46] a three-layer feedforward network of integrate-and-fire neurons with a STDP-like long-term potentiation window is used to produce a self-organised map of orientation preference, given appropriate receptive field shape and input properties. This map does not feature lateral connections or direct competition between neurons, instead relying on those receptive fields and input properties for the self-organisation to occur. As such, it is likely that an organised output map will only result from a limited range of inputs. The current approach can produce an output map based on organisation

to input data with any properties, due to the use of lateral connections for competition.

The LISSOM model has been modified to incorporate spiking neuron properties in [47], with Hebbian learning dependent on average activity rather than spike timing. This learning method is less biologically relevant than the STDP used in the current model, and using a network structure based on the visual system means that the map is not necessarily capable of mapping a wide variety of input data as in the current model and the conventional SOM.

In other recent work a pair of self-organising models have been presented that learn spatio-motor [48] and visual [49] representations using leaky integrate-and-fire neurons and STDP. Again, these models do not tackle the general problem addressed by the current model, but they are based on a shared core model which can be compared with the current method. This underlying model features Gaussian tuning of responsiveness to input properties, but using a firing-rate rather than spike-timing encoding. This leads to a slightly different role for STDP, in that it picks average pre- and postsynaptic combinations out of noisier activity, as opposed to being a method for storing phase-of-firing relationships in the current model. The visual representation model [49] has separate STDP rules for excitatory and inhibitory synapses in the 'map' layer. The inhibitory plasticity is found to be crucial for emergence of the representations, while preventing recurrent excitation from increasing firing rates. The current model avoids this through control of the relationship between maximum synaptic strength and number of neurons, but this method warrants investigation for automatic control of these properties in SOMs of different scales.

Each of these models suggest ways in which spiking neuron models can facilitate self-organisational network properties, but none of them represents a solution that incorporates the ideas of temporal coding of input data through relative phases of spikes within oscillations, continuous presentation of input data points to the network, and learning via STDP simultaneously. In addition, none of these models present a network structure possessing self-organisational and classification properties comparable with the traditional SOM algorithm.

##### B. Mechanisms, limitations and future directions

The inhibitory mechanism introduced to produce oscillatory firing with phase-of-firing coding from a continuously presented input activity level (see section II-C1) is a versatile and useful neural function in its own right. A drawback is that it is necessary to pre-determine the required size of a gap in the input pattern that will allow the inhibitory neuron to fire and the length and magnitude of the inhibition, which controls the rate of oscillation, by setting PSP values in (2) and (3). These values do not require rigorous fine-tuning provided the range of input activity levels across the pool of input neurons is relatively low, such that all neurons in the pattern will fire within a restricted time period, followed by a gap before the neuron with the strongest input will fire again. Additionally, it is also necessary to predetermine the strength of feedforward connections between the layers when the number of input

neurons changes. Currently there is no general method for deriving maximum weight values for different network scenarios, and the development of such a method would represent an important step towards a generalised spiking SOM.

Crucial future research will revolve around establishing more precisely the extent of the qualities of self-organisation that the spiking SOM possesses. It is currently unclear exactly how well the network can reorganise to shifting, non-stationary inputs, either varying distributions of a continuous multi-dimensional space, or in the form of correct incorporation and classification of additional input categories introduced after the network has been allowed to learn for some time. It can be speculated that the network will respond well to these challenges, a claim supported by the impressive ability of the network to accurately model input distributions and to adjust to one change in input data during training, results demonstrated in section III-D. A more detailed comparison of the capabilities of the current network with the capabilities of the conventional SOM would also require the introduction of analytical techniques that can assess more features of the mapping than the topographic representation. Measures such as quantisation error can assess whether a minimum distance from input patterns to their respective output layer representatives is achieved, and integrated measures, such as CQoCO, incorporate the extent to which nodes map regions from outside of the desired input space and the twistedness of the representation as it untangles throughout training into the quality of mapping metric [36].

Additional future research could also improve on the biological plausibility of the network structure and connection profile by basing these on knowledge of cortical areas. The current model is not based on a specific brain region, but the all-to-all connectivity used between layers is not seen in cortex, so represents a deviation from the way in which cortical functions are generated. As introduced in section IV-A, other work on self-organisation with spiking neurons has focused on generating maps using specific brain regions as inspiration. A synthesis of those approaches with the current one could lead to biologically plausible models with increased functionality and versatility in the future.

The use of phase-of-firing coding and an STDP learning rule has some limitations in the current context. Synaptic connections from neurons involved in the input pattern are weakened if the neuron fires late within the temporal sequence (i.e., after firing in the output layer). However, a neuron with much lower input activity would not fire at all for the current input; with STDP learning, synaptic connections from such neurons to the input layer are not weakened. This problem is not relevant if the input neurons that have connections to an output map represent a narrow domain of actual input stimuli, in which case any stimulus from the associated domain presented to that bank of input neurons would generate some relatively high activity level (and therefore firing) for the entire bank of neurons. Also, if output neurons have connections from input neurons that never fire in correlation with the dominant banks of input neurons connected to an output neuron, there is a chance that spontaneous activity would gradually weaken the connection, although the current model

does not support this.

A second problem with the use of phase coded input is that hierarchical layers of these SOMs are not possible. Output representation is spatial, within a relatively narrow temporal window. The same learning rule will not work if the SOM output is taken as input to a downstream SOM layer. Spreading the firing in the SOM layer into a temporal code (for example by adjusting synaptic time constants) would cause the self-organisation to fail, as neighbouring neurons in the output layer need to fire in close temporal proximity to ensure their weights are adjusted towards the same point. Of course, multiple independent SOMs could be set up with a temporal sequence between the SOMs, which could become input to a downstream SOM layer, creating a multi-modal association/integration of spatially coded features.

This type of spiking neuron network has the potential to be used to explore the connectivity and learning mechanisms involved in formation of networks analogous to cortical maps that display topological organisational structures, in artificial intelligence mechanisms that perform tasks like clustering, categorisation and concept formation in a biologically plausible manner, and in the development of spiking neuron hardware that physically represents neurons and networks in digital or analogue circuits.

## REFERENCES

- [1] J. H. Kaas and K. C. Catania, "How do features of sensory representations develop?," *BioEssays*, vol. 24, pp. 334–343, 2002.
- [2] B. A. Wandell, "The neurobiological basis of seeing words," *Annals of the New York Academy of Sciences*, vol. 1224, pp. 63–80, 2011.
- [3] V. A. Casagrande and J. H. Kaas, "The afferent, intrinsic, and efferent connections of primary visual cortex in primates," *Cerebral Cortex*, vol. 10, pp. 201–259, 1994.
- [4] J. C. Horton and D. R. Hocking, "Anatomical demonstration of ocular dominance columns in striate cortex of the squirrel monkey," *The Journal of Neuroscience*, vol. 16, no. 17, pp. 5510–5122, 1996.
- [5] G. G. Blasdel and G. Salama, "Voltage-sensitive dyes reveal a modular organization in monkey striate cortex," *Nature*, vol. 321, pp. 579–585, 1986.
- [6] D. H. Hubel, T. N. Wiesel, and M. P. Stryker, "Anatomical demonstration of orientation columns in macaque monkey," *The Journal of Comparative Neurology*, vol. 177, pp. 361–380, 1978.
- [7] M. M. Merzenich, P. L. Knight, and G. L. Roth, "Representation of cochlea within primary auditory cortex in the cat," *Journal of Neurophysiology*, vol. 38, no. 2, pp. 231–249, 1975.
- [8] X. Chen, M. Gabitto, Y. Peng, N. J. P. Ryba, and C. S. Zuker, "A gustotopic map of taste qualities in the mammalian brain," *Science*, vol. 333, pp. 1262–1266, 2011.
- [9] F. Wang, A. Nemes, M. Mendelsohn, and R. Axel, "Odorant receptors govern the formation of a precise topographic map," *Cell*, vol. 93, pp. 47–60, 1998.
- [10] T. A. Woolsey, C. Welker, and R. H. Schwartz, "Comparative anatomical studies of the SmL face cortex with special reference to the occurrence of "barrels" in layer IV," *Journal of Comparative Neurology*, vol. 164, pp. 79–94, 1975.
- [11] K. Fox, *Barrel Cortex*. Cambridge University Press, 2008.
- [12] R. M. Friedman, L. M. Chen, and A. W. Roe, "Modality maps within primate somatosensory cortex," *Proceedings of the National Academy of Sciences*, vol. 101, no. 34, pp. 12724–12729, 2004.
- [13] D. E. Feldman and M. Brecht, "Map plasticity in somatosensory cortex," *Science*, vol. 310, pp. 810–815, 2005.
- [14] M. M. Merzenich, J. H. Kaas, J. Wall, R. J. Nelson, M. Sur, and D. Felleman, "Topographic reorganization of somatosensory cortical areas 3b and 1 in adult monkeys following restricted deafferentation," *Neuroscience*, vol. 8, pp. 33–55, 1983.
- [15] M. B. Calford, "Dynamic representational plasticity in sensory cortex," *Neuroscience*, vol. 111, no. 4, pp. 709–738, 2002.

- [16] T. Kohonen, *Self-Organizing Maps*. Berlin Heidelberg New York: Springer-Verlag, third ed., 2001.
- [17] J. Hertz, A. S. Krogh, and R. G. Palmer, *Introduction to the Theory of Neural Computation*. Perseus Publishing, first ed., 1991.
- [18] E. T. Rolls and G. Deco, *Computational Neuroscience of Vision*. Oxford University Press, 2002.
- [19] N. Manukyan, M. J. Eppstein, and D. M. Rizzo, "Data-driven cluster reinforcement and visualization in sparsely-matched self-organizing maps," *IEEE Transactions on Neural Networks and Learning Systems*, vol. 23, no. 5, pp. 846–852, 2012.
- [20] C.-C. Hsu and S.-H. Lin, "Visualized analysis of mixed numeric and categorical data via extended self-organizing map," *IEEE Transactions on Neural Networks and Learning Systems*, vol. 23, pp. 72–86, Jan. 2012.
- [21] P. Maldonado, C. Babul, W. Singer, E. Rodriguez, D. Berger, and S. Grün, "Synchronization of neuronal responses in primary visual cortex of monkeys viewing natural images," *Journal of Neurophysiology*, vol. 100, pp. 1523–1532, 2008.
- [22] P. Fries, D. Nikolić, and W. Singer, "The gamma cycle," *Trends in Neurosciences*, vol. 30, no. 7, pp. 309–316, 2007.
- [23] S. J. Thorpe, D. Fize, and C. Marlot, "Speed of processing in the human visual system," *Nature*, vol. 381, pp. 520–522, 1996.
- [24] R. Van Rullen and S. J. Thorpe, "Rate coding versus temporal order coding: what the retinal ganglion cells tell the visual cortex.," *Neural Computation*, vol. 13, no. 6, pp. 1255–83, 2001.
- [25] T. K. Hensch, "Critical period regulation," *Annual Review of Neuroscience*, vol. 27, pp. 549–579, 2004.
- [26] B. Ruf and M. Schmitt, "Self-organization of spiking neurons using action potential timing," *IEEE Transactions on Neural Networks*, vol. 9, no. 3, pp. 575–578, 1998.
- [27] S. Song and L. F. Abbott, "Cortical remapping through spike timing-dependent plasticity," *Neuron*, vol. 32, pp. 1–20, 2001.
- [28] S. Song, K. D. Miller, and L. F. Abbott, "Competitive Hebbian learning through spike-timing-dependent synaptic plasticity," *Nature Neuroscience*, vol. 3, no. 9, pp. 919–926, 2000.
- [29] D. Bush, A. Philippides, P. Husbands, and M. O'Shea, "Reconciling the STDP and BCM models of synaptic plasticity in a spiking recurrent neural network," *Neural Computation*, vol. 22, pp. 2059–2085, 2010.
- [30] S. M. Bohte, H. La Poutré, and J. N. Kok, "Unsupervised clustering with spiking neurons by sparse temporal coding and multilayer RBF networks," *IEEE Transactions on Neural Networks*, vol. 13, no. 2, pp. 426–435, 2002.
- [31] X.-J. Wang, "Neurophysiological and computational principles of cortical rhythms in cognition," *Physiological Reviews*, vol. 90, pp. 1195–1268, 2010.
- [32] J. S. Law, *Modeling the development of organization for orientation preference in primary visual cortex*. PhD thesis, University of Edinburgh, 2009.
- [33] R. Keith-Magee, *Learning and development in Kohonen-style self-organising maps*. PhD thesis, Curtin University of Technology, 2001.
- [34] G. J. Goodhill and T. J. Sejnowski, "A unifying objective function for topographic mappings," *Neural Computation*, vol. 9, pp. 1291–1303, 1997.
- [35] D. Vidaurre and J. Muruzábal, "A quick assessment of topology preservation for SOM structures," *IEEE Transactions on Neural Networks*, vol. 18, pp. 1524–1528, Sept. 2007.
- [36] D. Beaton, I. Valova, and D. Maclean, "CQoCO: A measure for comparative quality of coverage and organization for self-organizing maps," *Neurocomputing*, vol. 73, pp. 2147–2159, 2010.
- [37] D. Polani, "Measures for the organization of self-organizing maps," in *Self-Organizing Neural Networks* (U. Seiffert and L. C. Jain, eds.), pp. 13–44, Berlin, Heidelberg: Physica-Verlag, Springer, 2002.
- [38] R. A. Fisher, "The use of multiple measurements in taxonomic problems," *Annals of Eugenics*, vol. 7, no. 2, pp. 179–188, 1936.
- [39] Q. Wu, T. McGinnity, L. Maguire, B. Glackin, and A. Belatreche, "Learning under weight constraints in networks of temporal encoding spiking neurons," *Neurocomputing*, vol. 69, pp. 1912–1922, 2006.
- [40] J. Wade, L. McDaid, J. Santos, and H. Sayers, "SWAT: a spiking neural network training algorithm for classification problems," *IEEE Transactions on Neural Networks*, vol. 21, no. 11, pp. 1817–1830, 2010.
- [41] N. Gueorgieva, I. Valova, and G. Georgiev, "Learning and data clustering with an RBF-based spiking neuron network," *Journal of Experimental & Theoretical Artificial Intelligence*, vol. 18, no. 1, pp. 73–86, 2006.
- [42] S.-Y. Yoon and S.-Y. Lee, "Training algorithm with incomplete data for feed-forward neural networks," *Neural Processing Letters*, vol. 10, no. 3, pp. 171–179, 1999.
- [43] L. Bako, "Real-time classification of datasets with hardware embedded neuromorphic neural networks," *Briefings in Bioinformatics*, vol. 11, no. 3, pp. 348–363, 2010.
- [44] D. M. Sala, K. J. Cios, and J. T. Wall, "Self-organization in networks of spiking neurons," *Australian Journal of Intelligent Information Processing Systems*, vol. 5, no. 3, pp. 161–170, 1998.
- [45] R. J. MacGregor, *Neural and Brain Modeling*. Academic Press, 1987.
- [46] F. Veredas, H. Mesa, and L. A. Martínez, "Imprecise correlated activity in self-organizing maps of spiking neurons," *Neural Networks*, vol. 21, pp. 810–816, 2008.
- [47] Y. Choe and R. Miikkulainen, "Self-organization and segmentation in a laterally connected orientation map of spiking neurons," *Neurocomputing*, vol. 21, pp. 139–157, 1998.
- [48] N. Srinivasa and Y. Cho, "Self-organizing spiking neural model for learning fault-tolerant spatio-motor transformations," *IEEE Transactions on Neural Networks and Learning Systems*, vol. 23, no. 10, pp. 1526–1538, 2012.
- [49] N. Srinivasa and Q. Jiang, "Somatosensory cortex: structural alterations following early injury to sense organs," *Frontiers in Computational Neuroscience*, vol. 7, no. 10, pp. 1–24, 2013.